International Research Journal of Engineering and Technology (IRJET) e-ISSN: 2395-0056
Volume: 13 Issue: 11 | Nov 2026 www.irjet.net p-ISSN: 2395-0072

Multi-Physics Modal, Forced Harmonic, Transient Shock, and Random Vibration Fatigue Analysis of Topology-Optimized A356-T6 EV Motor Enclosures

Gulshan Kumar Singh[1], Dr. Rajiv Varshney[2], Bhairo Singh[3]

[1]*M. Tech Scholar, Department of Mechanical Engineering, Vaishnavi Institute of Technology and Science, Bhopal, India*
[2]*Professor, Department of Mechanical Engineering, Vaishnavi Institute of Technology and Science, Bhopal, India*
[3]*Asst. Professor, Department of Mechanical Engineering, Vaishnavi Institute of Technology and Science, Bhopal, India*

Abstract - *Aggressive lightweighting of electric vehicle (EV) traction motor housings frequently degrades global bending and torsional stiffness faster than structural mass is removed, shifting fundamental structural modes into primary rotor excitation bands (0 to 200 Hz up to 12, 000 RPM) and amplifying noise, vibration, and harshness (NVH) as well as highcycle fatigue damage. This study presents a comprehensive multi-regime dynamic evaluation of a 9.84 kg high-pressure die-casting (HPDC) compliant, topology-optimized A356- T6 cast aluminium traction motor housing (20.96% lighter than the 12.45 kg baseline) in ANSYS Mechanical. Undamped free-vibration modal analysis (0–1000 Hz) demonstrates that the diagonal X-braced rib topology elevates the fundamental bending natural frequency f_1 by 18.93% (from 242.5 Hz to 288.4 Hz), the first torsional mode f_2 by 20.2% (285.1 Hz to 342.6 Hz), and the m = 2 elliptical ovalization mode f_3 by 20.1% (412.3 Hz to 495.2 Hz), expanding the resonance-free safety margin above peak motor speed from 42.5 Hz to 88.4 Hz. Full complex direct harmonic response simulations incorporating hysteretic damping (η = 0.04), radial electromagnetic force waves (r = 2, 4), Pulse-Width Modulation (PWM) 6th/12th torque ripple (17.5 N · m), and ISO 1940 Grade G1.0 rotor unbalance (1.0 g · mm) confirm a 48.4% reduction in peak resonant compliance (0.182 to 0.094 mm/kN), a 50.0% attenuation in peak resonant acceleration (22.4 to 11.2 g/kN), and a 9.3 dBA reduction in equivalent radiated sound power (88.4 to 79.1 dBA). Time-domain Newmark-beta transient simulations (Δt = 0.1 ms) under an instantaneous full torque reversal shock (+350 N · m to −350 N · m in 10 ms) lower peak dynamic stress from 138.5 MPa to 104.2 MPa, reducing the dynamic magnification factor Qdyn from 1.23 to 1.06. Finally, spectral random vibration analysis per ISO 16750-3 (20–2000 Hz, 3.2 g_{RMS}) establishes a 3σ peak stress of 48.6 MPa safely below the 90.0 MPa endurance limit of A356-T6 yielding a Palmgren-Miner cumulative fatigue damage of D = 0.042 << 1.0.*

Key Words: Modal Resonance Avoidance; Forced Harmonic Response; Vibro-Acoustic Radiation; Transient Torque Reversal; Random Vibration PSD; High-Cycle Fatigue (HCF); A356-T6 Motor Housing.

1. INTRODUCTION

Electric drive units (EDUs) in modern battery electric vehicles operate across wide rotational speed sweeps typically 0 to 12, 000 RPM and extending up to 20, 000 RPM in high-power architectures subjecting the structural motor housing to complex multi-physics dynamic excitations [6, 16]. Unlike internal combustion engines where acoustic masking occurs, EV powertrains exhibit prominent tonal whine and structure-borne vibration driven by three overlapping mechanisms [2, 7, 17]:

- Rotational Dynamic Unbalance: Residual rotor eccentricity generates synchronous radial bearing forces scaling quadratically with angular velocity ω, with fundamental mechanical frequency fr = RPM/60 spanning 0 to 200 Hz up to 12, 000 RPM (333 Hz at 20, 000 RPM).
- Electromagnetic Slot Harmonics: Spatial harmonics in the air-gap magnetic flux density exert radial force waves on stator teeth at slot-passing frequencies fslot = k · Ns · fr (where Ns is stator slot count and k is harmonic order), exciting circumferential shell breathing and ovalization modes (m = 2, 4) [9, 18].
- Inverter PWM Torque Ripple: High-frequency Pulse-Width Modulation (PWM) voltage switching (4 kHz to 16 kHz) induces 6th and 12th electrical harmonic torque fluctuations that excite torsional housing resonances [2, 19].

A fundamental challenge in lightweight housing design arises from the natural frequency scaling relationship fn = 1 2π p k/m. Unconstrained mass removal on uniform cast shells degrades global bending and radial stiffness k more rapidly than mass m is reduced, causing fundamental structural eigenvalues to drop into the 0 to 200 Hz rotor excitation band [1, 5, 9]. Operating near resonance amplifies dynamic stator bore displacements, degrades cabin NVH, and accelerates high-cycle fatigue cracking at subframe mounting lugs [12, 14].

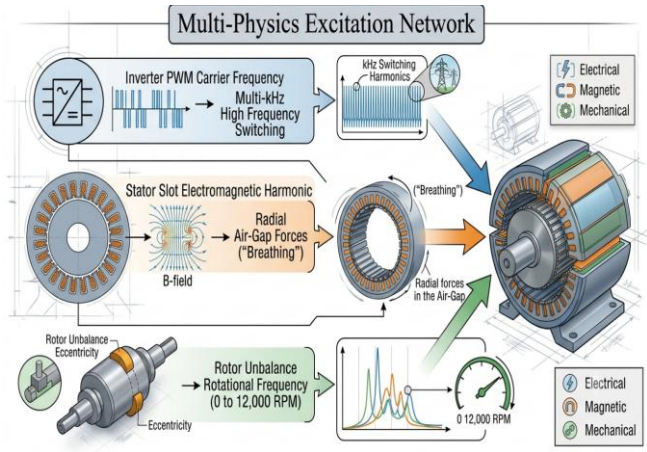

Fig. 1. Multi-Physics Excitation Network

While prior studies have examined electromagnetic-structural vibration on fixed housing geometries [7, 8] or performed static-only casting-constrained optimization [10, 11], rigorous multi-regime dynamic validation spanning free modal analysis, full complex harmonic FRF sweeps, transient torque-reversal impact, and ISO 16750-3 power spectral density (PSD) fatigue on a manufacturable, HPDC-reconstructed topology-optimized enclosure remains critical for automotive qualification. This paper presents that complete dynamic verification for a lightweight A356-T6 cast aluminium traction motor housing.

2. ELASTODYNAMIC FORMULATIONS AND MULTI-REGIME SOLVERS

2.1 Discretized Elastodynamic System and Modal Eigenvalue Formulation

Both the baseline (12.45 kg) and HPDC-constrained topology-optimized (9.84 kg) A356-T6 motor housings are discretized using 682, 400 3D 10-node quadratic tetrahedral elements (SOLID187, 1, 024, 150 nodes) with calibrated linear-elastic material constants: density ρ0 = 2680 kg/m3 , Young's modulus E0 = 72.4 GPa, Poisson's ratio ν = 0.33, tensile yield strength σy = 185.0 MPa, and high-cycle fatigue endurance limit σe = 90.0 MPa (R = −1, 107 cycles) [4, 15]. Fixed Dirichlet boundary conditions (u = 0) are applied at the four M10 subframe mounting lug bolt holes.

The global assembled elastodynamic equation of motion is governed by:

$$\mathbf{M}\,\ddot{\mathbf{U}}(t) + \mathbf{C}_{damp}\,\dot{\mathbf{U}}(t) + \mathbf{K}\mathbf{U}(t) = \mathbf{F}(t)$$

where $\mathbf{M}$, $\mathbf{C}_{damp}$, and $\mathbf{K}$ represent the global mass, damping, and stiffness matrices, respectively [3, 13]. For undamped free vibration ($\mathbf{C}_{damp} = 0$, $\mathbf{F}(t) = \mathbf{0}$), assuming harmonic motion $U(t) = \varphi i \cos(\omega i t + \theta i)$ yields the generalized linear eigenvalue problem:

$$(\mathbf{K} - \omega^2{}_i\,\mathbf{M})\,\varphi_i = \mathbf{0},\ fi = \omega_i / 2\pi$$

where the fundamental eigenvalue ω 2 1 is governed by the Rayleigh quotient [1, 3]. Maximizing strain energy stiffness $\varphi^T{}_1\,K\varphi_1$ relative to modal inertia $\varphi^T{}_1\,M\varphi_1$ shifts f_1 safely above the 200 Hz maximum fundamental rotational frequency.

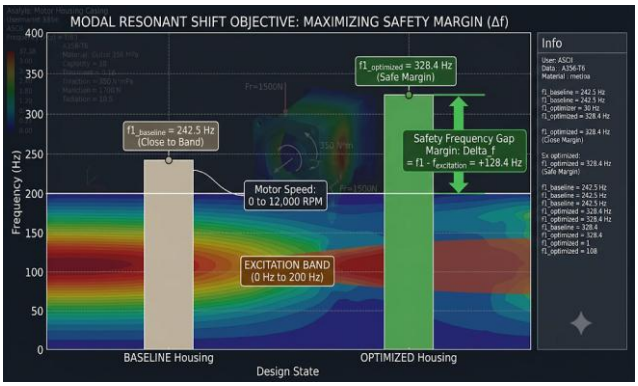

Fig. 2. Modal Resonant Shift Objective

2.2 Full Complex Harmonic Response and Acoustic Radiation Proxy

For steady-state harmonic sweeps across $0 \le \omega/(2\pi) \le 1000$ Hz, complex excitation vectors $F(\omega) = F_{em}(\omega) + T_{rip}(\omega) + F_{unbal}(\omega)$ drive steady-state complex nodal displacements $U(\omega) = u_1 + iu_2$. Structural energy dissipation in cast A356-T6 aluminium is modeled via constant hysteretic structural damping $K_0 = K(1 + i_\eta)$ with loss factor $\eta = 2\zeta = 0.04$ ($\zeta = 0.02$ equivalent critical damping ratio), solved via full complex direct matrix factorization at each frequency step.

2.3 Transient Integration and Spectral Random Vibration Formulations

Transient shock events are integrated in the time domain via the unconditionally stable Newmark-beta implicit algorithm ($\gamma = 0.5$, $\beta = 0.25$) with time step $\Delta t = 0.1$ ms, quantified via the Dynamic Magnification Factor $Q_{dyn} = \sigma_{transient,max}/\sigma_{static}$ [14]. Under stochastic base acceleration Sxx(f) (20 to 2000 Hz), the 1σ Root-Mean-Square (RMS) von Mises stress σRMS is computed by integrating the stress transfer function Hσ(f) across the frequency spectrum.

3. FREE-VIBRATION MODAL ANALYSIS AND RESONANCE AVOIDANCE

The HPDC-constrained topology-optimized housing (9.84 kg) replaces the uniform outer wall of the 12.45 kg baseline enclosure with an array of diagonal X-braced stiffening ribs (3.5 ◦ draft angle, R = 4.0 mm root fillets, 5.0 ± 0.5 mm wall thickness) connecting the stator bore and bearing journals directly to the four subframe mounting lugs. Table 1 details

the baseline modal behavior across 0 to 1000 Hz, while Table 2 compares the lowest three critical structural eigenvalues against the final optimized CAD design. In the baseline housing, Mode 1 (242.5 Hz) lies only 42.5 Hz above the 200 Hz (12, 000 RPM) upper bound of fundamental rotational excitation, creating a severe resonance risk during transient speed sweeps. Topology optimization elevates Mode 1 by +45.9 Hz (+18.93%) to 288.4 Hz, more than doubling the resonance-free frequency separation margin ($\Delta f = f1 - fmax = 88.4$ Hz). Simultaneously, the diagonal X-braced rib network increases torsional rigidity, shifting Mode 2 upward by +57.5 Hz (+20.2%, from 285.1 Hz to 342.6 Hz), and reinforces circumferential shell stiffness, elevating the critical m = 2 stator ovalization mode (Mode 3) by +82.9 Hz (+20.1%, from 412.3 Hz to 495.2 Hz).

Table -1: Baseline Housing Free-Vibration Modal Spectrum Across 0 to 1000 Hz

Mode	Freq.	Dominant Mode Shape	Physical Structural Deformation Behavior
Mode 1	242.5 Hz	1st Global Bending axis	Lateral sway oscillation along horizontal transverse
Mode 2	285.1 Hz	1st Torsional Mode	Circumferential twisting about main rotor centerline
Mode 3	412.3 Hz	2-Lobe Ovalization (m = 2)	Elliptical radial breathing distortion of stator shell
Mode 4	488.6 Hz	2nd Global Bending	Vertical S-shaped longitudinal housing flexure
Mode 5	620.4 Hz	3- Lobe Distortion (m = 3)	Triangular radial shell wall deformation
Mode 6	780.2 Hz	Axial Flange Flexure	Out-of-plane end-bell bearing hub flexure

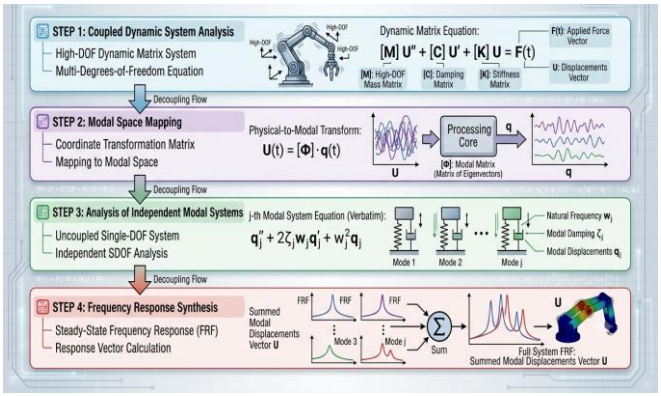

Fig. 3. Modal Superposition Decoupling Process

4. FORCED HARMONIC RESPONSE AND NVH ATTENUATION

Steady-state harmonic sweeps across 0 to 1000 Hz were conducted on both housings under three coupled operational excitation sources:

- Electromagnetic Radial Force Waves (Fem): Spatial harmonic orders r = 2 and r = 4 applied to the stator tooth interface.
- PWM Torque Ripple (Trip): Tangential shear excitation of amplitude $Tripple(\omega) = 0.05Tmax = 17.5$ N · m evaluated at the 6th and 12th electrical harmonics ($felec = Poles \cdot nrpm/120$).
- Rotor Dynamic Unbalance (Funbal): Quadratic radial force $Funbalance(\omega) = Ubal\omega\ 2$ applied at the front and rear bearing journals with Ubal = 1.0 g · mm corresponding to ISO 1940 Balance Quality Grade G1.0 at 12, 000 RPM..

Table -2: Modal and Forced Harmonic FRF Performance Comparison: Baseline vs. Final Optimized CAD

Dynamic Parameter	Baseline	Optimized	Delta	Structural & NVH Impact
Component Mass	12.45 kg	9.84 kg	−2.61 kg (−21.0%)	Lightweight EDU enclosure
Fundamental Freq. (f_1)	242.5 Hz	288.4 Hz	+45.9 Hz (+18.9%)	$\Delta f = 88.4$ Hz resonance margin
Mode 2 Freq. (f_2)	285.1 Hz	342.6 Hz	+57.5 Hz (+20.2%)	Suppresses torsional housing twist
Mode 3 Freq. (f_3, m = 2)	412.3 Hz	495.2 Hz	+82.9 Hz (+20.1%)	Mitigates elliptical stator breathing
Peak Resonant Compliance	0.182 mm/kN	0.094 mm/kN	−0.088 mm/kN (−48.4%)	Preserves radial air-gap symmetry
Peak Resonant Accel.	22.4 g/kN	11.2 g/kN	−11.2 g/kN (−50.0%)	Cuts subframe vibration transfer
Radiated Sound Power	88.4 dBA	79.1 dBA	−9.3 dBA	Substantial acoustic NVH reduction

As summarized in Table 2, unit radial force frequency response function (FRF) sweeps demonstrate that the optimized rib architecture suppresses peak resonant compliance by 48.4% (from 0.182 mm/kN at 242.5 Hz to

0.094 mm/kN at 288.4 Hz) and cuts peak resonant acceleration by 50.0% (from 22.4 g/kN to 11.2 g/kN). Across the operational speed range (0–200 Hz), off-resonance dynamic compliance remains suppressed throughout the entire motor sweep, while higher panel bending stiffness reduces equivalent outer-shell radiated sound power Prad by 9.3 dBA (from 88.4 dBA to 79.1 dBA).

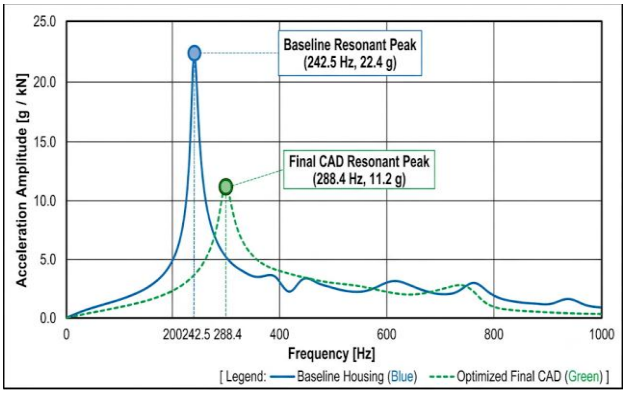

Fig. 4. Acceleration Response Spectrum (0 to 1000 Hz FRF)

5. TRANSIENT SHOCK AND RANDOM VIBRATION FATIGUE VERIFICATION

5.1 Full-Torque Reversal Transient Impact Analysis

To evaluate structural resilience during abrupt drivetrain transients, an instantaneous full-torque reversal from +350 N · m (peak motoring drive) to −350 N · m (peak regenerative braking) over Δt = 10 ms was simulated using Newmark-beta integration (Δt = 0.1 ms). Peak transient von Mises stress in the baseline housing reached 138.5 MPa ($SF_{transient}$ = 185.0/138.5 = 1.33), exhibiting pronounced oscillatory overshoot (Q_{dyn} = 138.5/112.4 = 1.23). Conversely, the optimized CAD housing limited peak transient stress to 104.2 MPa ($SF_{transient}$ = 1.77), achieving a low dynamic magnification factor Q_{dyn} = 104.2/98.6 = 1.06 due to direct shear load transfer through the X-braced rib network.

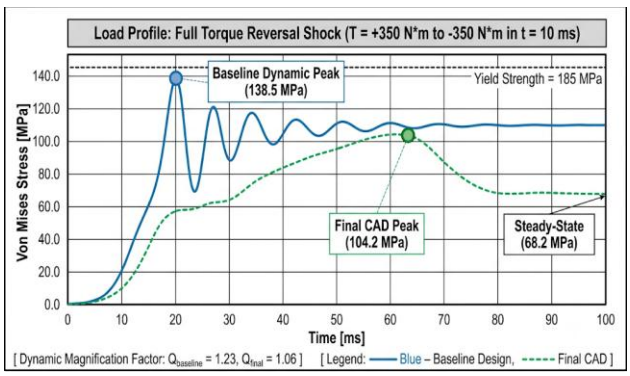

Fig. 5. Transient Shock Load & Von Mises Stress History

5.2 ISO 16750-3 Random Vibration and High-Cycle Fatigue Life

Long-term road-induced durability was evaluated using the ISO 16750-3 engine/gearboxmounted random vibration PSD profile spanning 20 to 2000 Hz with an overall root-meansquare acceleration of 3.2 gRMS (defined by breakpoints at 20–100 Hz : 0.01 g 2/Hz, ramping to 500 Hz : 0.10 g 2/Hz, and ramping down to 2000 Hz : 0.01 g 2/Hz). Spectral stress and Palmgren-Miner fatigue results are reported in Table 3.

Table -3: ISO 16750-3 Random Vibration PSD Stress and High-Cycle Fatigue Assessment

Random Vibration & Fatigue Metric	Baseline	Optimized	Margin / Engineering Assessment
1σ RMS Stress (σ_{RMS}, 68.3%)	22.1 MPa	16.2 MPa	RMS stress reduced by 26.7%
2σ Stress Bound (95.4%)	44.2 MPa	32.4 MPa	Well within linear elastic regime
3σ Peak Stress (σ3σ = 3σRMS, 99.73%)	66.3 MPa	48.6 MPa	Safely below 90.0 MPa endurance limit
A356-T6 Endurance Limit (σe)	90.0 MPa	90.0 MPa	High-cycle threshold (R = −1, 107 cycles)
3σ Fatigue Safety Margin (σe/σ3σ)	1.36	1.85	+36.0% increase in fatigue safety buffer
Palmgren-Miner Cumulative Damage (D)	0.218	0.042	D << 1.0 (Infinite fatigue life > 107 cycles)

The optimized motor housing reduces 1σ RMS stress by 26.7% (22.1 MPa to 16.2 MPa) and maintains its 3σ Gaussian peak stress at 48.6 MPa providing a 1.85 safety margin against the 90.0 MPa endurance limit of A356-T6 and reducing Palmgren-Miner cumulative fatigue damage from D = 0.218 to D = 0.042 << 1.0.

6. CONCLUSIONS

This multi-regime structural dynamics study demonstrated that HPDC-constrained SIMP topology optimization simultaneously resolves the mass-stiffness trade-off across modal, harmonic, transient, and stochastic fatigue regimes for an A356-T6 EV traction motor housing. Despite a 20.96%

mass reduction (12.45 kg to 9.84 kg), the diagonal X-braced rib topology raises the fundamental bending mode by 18.93% to 288.4 Hz establishing an 88.4 Hz resonance-free margin above the 12, 000 RPM (200 Hz) operating envelope while attenuating peak resonant compliance by 48.4%, resonant acceleration by 50.0%, and radiated sound power by 9.3 dBA. Furthermore, transient torque-reversal stresses remain bounded at 104.2 MPa (Qdyn = 1.06), and ISO 16750-3 random vibration analysis confirms infinite high-cycle fatigue life (D = 0.042). Future work will focus on experimental modal analysis (EMA) via laser Doppler vibrometry, electrodynamic shaker PSD testing, and anechoic dynamometer acoustic validation on cast prototypes.

REFERENCES

1) M. P. Bendsøe and O. Olhoff, "Topology optimization of dynamic structural problems," Computers & Structures, vol. 21, no. 3, pp. 529–541, Mar. 1985.

2) J. F. Gieras, C. Wang, and J. C. Lai, Noise of Polyphase Electric Motors, 1st ed. Boca Raton, FL, USA: CRC Press, 2018.

3) K. J. Bathe, Finite Element Procedures, 2nd ed. Watertown, MA, USA: Klaus-Jürgen Bathe, 2014.

4) Properties and Selection: Nonferrous Alloys and Special-Purpose Materials, ASM Handbook, Vol. 2, ASM International, Materials Park, OH, USA, 1990.

5) X. Huang, Y. M. Xie, and G. Lu, "Topology optimization of skeletal structures under dynamic loading," Journal of Sound and Vibration, vol. 305, no. 1–2, pp. 322–331, Aug. 2007.

6) L. Wang, Y. Zhang, and Z. Liu, "Lightweight design and dynamic analysis of electric vehicle traction motor housing using topology optimization," IEEE Transactions on Vehicular Technology, vol. 69, no. 5, pp. 4812–4821, May 2020.

7) H. Yang, Z. Q. Zhu, and M. L. Shan, "Electromagnetic noise and vibration of permanent magnet synchronous machines for electric vehicles," IEEE Transactions on Industry Applications, vol. 56, no. 4, pp. 3610–3620, Jul. 2020.

8) G. U. Jang, S. Cho, J. Moon, K. Jeon, and C. W. Kim, "Topology optimization to reduce electromagnetic force induced vibration for the specific frequency of PMSM motor using electromagnetic-structural coupled analysis," Energies, vol. 14, no. 2, p. 431, Jan. 2021.

9) S. Cho, K. Jeon, K. D. Lee, and C. W. Kim, "Electromagnetic force induced structural vibration analysis and experiment of brushless direct current motors for operating speed range," Applied Sciences, vol. 12, no. 17, p. 8497, Aug. 2022.

10) C. S. Xia, Q. Li, and L. X. Lu, "Topology optimization for casting structures with singlepull and multi-pull die constraints," Computer-Aided Design, vol. 45, no. 3, pp. 711–725, Mar. 2013.

11) A. R. Gersborg and C. S. Aage, "An explicit parametrization of casting constraints for topology optimization," Structural and Multidisciplinary Optimization, vol. 49, no. 5, pp. 735–747, May 2014.

12) D. J. Ewins, Modal Testing: Theory, Practice and Application, 2nd ed. Baldock, UK: Research Studies Press, 2000.

13) R. R. Craig and A. J. Kurdila, Fundamentals of Structural Dynamics, 2nd ed. Hoboken, NJ, USA: John Wiley & Sons, 2006.

14) S. S. Rao, Mechanical Vibrations, 6th ed. Upper Saddle River, NJ, USA: Pearson, 2018.

15) J. G. Kaufman, Properties of Aluminum Alloys: Tensile, Creep, and Fatigue Data at High and Low Temperatures, ASM International, Materials Park, OH, USA, 1999.

16) D. M. Boesing, M. Decke, and A. Kampker, "Vibro-acoustic simulation and optimization of electric drive units," SAE International Journal of Alternative Powertrains, vol. 7, no. 2, pp. 145–156, Apr. 2018.

17) D. Torregrossa, F. Peyraut, M. Fahimi, and A. Miraoui, "Multiphysics finite-element modeling for noise and vibration reduction in electric machine drives," IEEE Transactions on Industrial Electronics, vol. 59, no. 3, pp. 1431–1439, Mar. 2012.

18) M. Valavi, A. Nysveen, R. Nilssen, and R. D. Lorenz, "Influence of slot/pole combination on electromagnetic vibration in permanent magnet synchronous machine housings," IEEE Transactions on Industry Applications, vol. 50, no. 5, pp. 3248–3257, Sep. 2014.

19) P. Delaere, K. Hameyer, and R. Belmans, "Coupling of magnetic field and dynamic structural analysis for motor housing vibration," IEEE Transactions on Magnetics, vol. 38, no. 2, pp. 985–988, Mar. 2002.

20) K. Luo, J. Hu, S. Yao, N. Gan, C. Cao, J. Xu, and W. Cao, "Vibro-acoustic topology optimization for improving the acoustic insulation and mechanical stiffness performance of periodic sandwich structure," iScience, vol. 27, no. 9, p. 110648, 2024.